

A Smartphone-Based Fourier Ptychographic Microscope Using the Display Screen for Illumination

Kyung Chul Lee, Kyungwon Lee, Jaewoo Jung, Se Hee Lee, Donghyun Kim, and Seung Ah Lee*



Cite This: *ACS Photonics* 2021, 8, 1307–1315



Read Online

ACCESS |

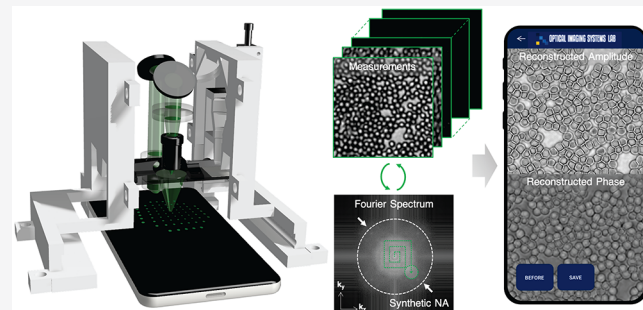
Metrics & More

Article Recommendations

Supporting Information

ABSTRACT: We propose a smartphone-mountable computational microscope that achieves wide-field and high-resolution imaging, based on the Fourier ptychographic (FP) microscopy technique. Our device uses the smartphone's built-in camera for microscopy imaging, the display screen for programmable illumination, and the computational power of the smartphone processors for FP image reconstruction. With a compact and lightweight optics module and a custom-built application, we can transform a regular smartphone into a high-performance microscope device with a space-bandwidth product exceeding that of regular benchtop microscopes. Our device achieves a half-pitch resolution of 870 nm over a wide field-of-view of $2.1 \times 1.6 \text{ mm}^2$ with amplitude, phase, and color imaging capabilities. We report on the design of the illumination and imaging system, our methods for fast FP reconstruction on the smartphone microscope, and the performance of the device. Using various clinical samples, we also discuss the potential of our device for clinical applications in resource-limited settings.

KEYWORDS: *smartphone microscopy, Fourier ptychographic microscopy, portable microscopy, programmable illumination, computational imaging*



The reduction of the size and cost of microscopes creates new possibilities for disease screening and health care in resource-limited settings. Smartphones and mobile devices can be useful for the construction of compact and portable imaging devices, by replacing expensive and bulky optical instruments with state-of-the-art cameras, high-performance processors, and network connectivity in a compact footprint. The rapid dissemination of smartphones and their user-friendly interfaces can allow for microscopic imaging and evaluation of biological specimens to be accessible to the general public as well as trained health care professionals. As the technologies for image sensors, miniaturized optics, and mobile processors continue to develop, these smartphone-enabled devices are expected to change how medical tests and evaluations are conducted in the field, as well as in the lab.

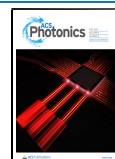
By leveraging the advanced capabilities of mobile devices, increasing efforts have been made to create portable microscopes for field applications.^{1–10} In earlier demonstrations of mobile phone microscopes, regular microscope optics were connected to the built-in camera modules to demonstrate portable imaging devices.¹ Designs using short-focal-length lenses placed in the vicinity of the camera lens,^{2,3,11} as well as lens-free microscopy techniques, such as shadow imaging and inline holography,^{4,5} have subsequently been adopted to realize compact and hand-held microscopes using smartphones. Other microscopy modalities such as fluorescence and phase/phase-contrast microscopy have also been implemented on

smartphones using separate LED-based modules as the illumination source.^{6–8} These various demonstrations have successfully shown the potential of portable imaging devices for diagnostic applications in the field, including the detection of bacterial infections and waterborne pathogens and the diagnosis of blood-borne diseases.^{9,10,12–14}

However, despite the efforts, most low-cost portable microscopes that use smartphone cameras offer a limited optical resolution and field-of-view (FOV) compared with the lab-based gold-standard equipment. In general, smartphone cameras are designed for wide-field photography, incorporating small-pixel image sensors and miniature lens modules with large chief ray angles (CRA) at the outer regions of the image sensor. The addition of a microscope on top of these camera modules results in severe vignetting or a limited FOV due to the finite aperture of the microscope.² In addition, the use of low-cost optics usually causes severe aberrations, making it difficult to achieve a high optical resolution throughout the entire FOV. For these reasons, the space-bandwidth product

Received: March 7, 2021

Published: April 23, 2021



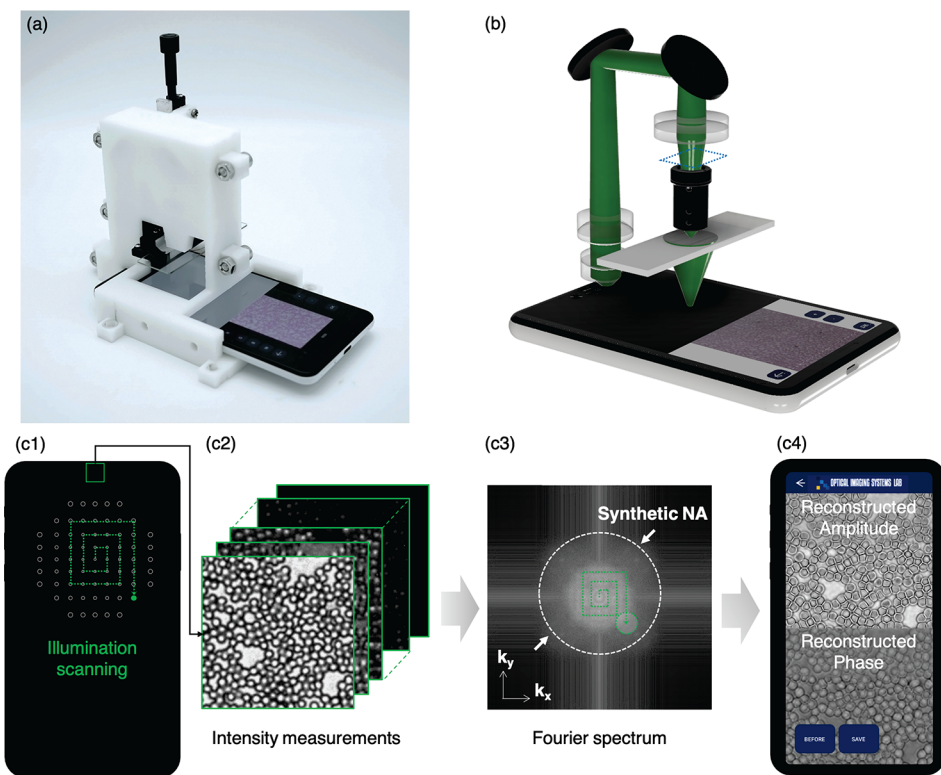


Figure 1. Overview of the proposed smartphone microscope. (a) Photograph of the smartphone-based FPM device in action. (b) Overall optical configuration of the microscope using the front camera module for imaging and the display screen as the illumination source. (c) The working principle of the proposed smartphone FPM, where multiple LR images are captured with scanning illumination and then reconstructed into HR amplitude and phase images in the smartphone.

(SBP) of smartphone-based microscopes has been limited and has not been taking full advantage of the large pixel counts of the state-of-the-art consumer-grade image sensors. The SBP is a measure of the information content of the imaging system and is directly associated with the diagnostic or screening capabilities of the microscope. The conventional methods for increasing the SBP, such as the use of sample scanning or large aperture optics, increases the cost, complexity, and size of the imaging system, which is not desirable for field applications. Furthermore, while lens-free methods can achieve a large SBP with computational image reconstruction, these methods require a dedicated device for the microscope as the camera module has to be significantly modified.^{4,5}

In the field of microscopy, various computational imaging techniques have been recently developed to effectively maximize the SBP and the amount of information content of the imaging systems.^{4,15,16} In particular, Fourier ptychographic microscopy (FPM) allows for achieving high-resolution (HR) and wide-field imaging by computationally combining a number of low-resolution (LR) images illuminated from different incident angles into a single HR image.¹⁵ A typical FPM setup involves the use of a low numerical aperture (NA) objective lens for wide-field imaging and a LED matrix for increasing the synthetic NA of the system, which effectively increases the SBP of the microscope without any mechanical scanning. The Fourier ptychography (FP) reconstruction is based on the Fourier optics-based forward model and the iterative phase retrieval, which recovers the sample's complex field information in HR and permits both bright-field and quantitative phase microscopy.¹⁷ Various additional techniques, including embedded pupil recovery (EPRY) for

aberration correction,¹⁸ illumination multiplexing,¹⁹ and illumination optimization,^{20,21} as well as deep-learning-based approaches for reconstruction,²² have been applied to FPM in order to increase both the reconstruction quality and processing speed. With ultrawide-field imaging capabilities far exceeding the SBP of regular microscopes, FPM has emerged as a powerful imaging tool for biological and clinical applications, including digital pathology, cytology, and high-throughput screening.^{23,24}

In this work, we propose a low-cost, field-portable FPM on a smartphone for imaging applications in resource-limited settings (Figure 1). Our device uses the front camera module of a smartphone for image acquisition and the display screen as the illumination source for the FPM and performs *in situ* image reconstruction using the smartphone's processors. The use of an organic LED (OLED) screen as the programmable illumination source allows for a compact device form factor while providing a large degree of freedom for illumination engineering for FP reconstruction. To utilize both the screen and the camera, we designed a phone-mountable 3D-printed microscope module with low-cost and off-the-shelf optical components and developed an Android application for imaging. This way, our method can transform any regular smartphone into a stand-alone, wide-field microscope without any modification of the device or additional electronics. In the following sections, we report on the design of the illumination and imaging hardware, the methods for FP reconstruction in our microscope, and the performance of the device. In the process, we demonstrate the workflow of our device with examples of the reconstructed images and discuss the potential of our device for field diagnostic applications.

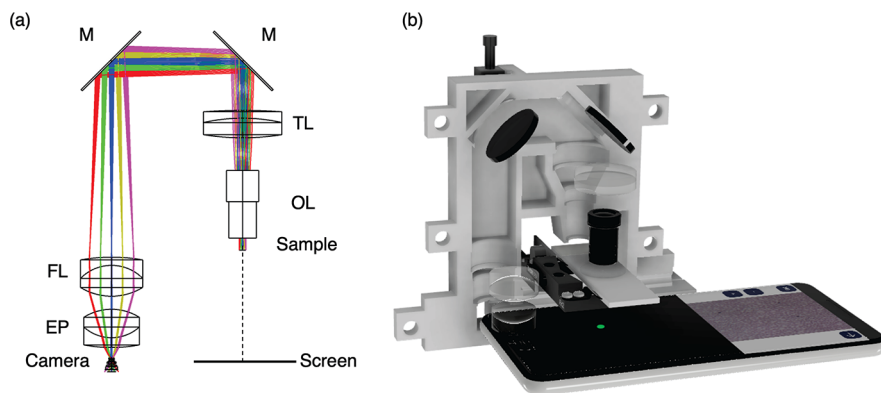


Figure 2. Design of the compact FPM module on a smartphone. (a) Optical layout of the microscope module (OL, objective lens; TL, tube lens; M, mirror; FL, field lens; EP, eyepiece lens). (b) Illustration of the assembled microscope module and the housing for mounting the smartphone.

METHODS

FPM is a computational microscopy technique that enhances the effective NA of the imaging system by using multiple images illuminated from different angles of incidence.¹⁵ Under the thin-sample assumption, changing the illumination angle is equivalent to rotating the angular spectrum of the object wave about the optical axis of the imaging system. Each LR image represents the intensity of the object's spectrum, shifted by the illumination wavevector and collected by the limited NA of the objective lens. The object's spatial information encoded in the LR image sequence is combined in the Fourier domain to recover the HR image of the object. In this process, the complex field of the object can be recovered.

The forward model of FPM can be mathematically modeled using Fourier optics. If the object is sufficiently thin, the transmittance of the object can be modeled as $o(\mathbf{r}) = e^{-\mu(\mathbf{r})+i\phi(\mathbf{r})}$, where $\mu(\mathbf{r})$ and $\phi(\mathbf{r})$ denote the absorbance and phase delay of the object in 2D spatial coordinates $\mathbf{r} = (x, y)$. When illuminated with the m th LED in the matrix, the LED is modeled as a spatially coherent monochromatic light source with an illumination wavevector \mathbf{k}_m , and the resulting exit light field can be modeled as $e(\mathbf{r}) = o(\mathbf{r}) e^{i\mathbf{k}_m(\mathbf{r})}$ or $E(\mathbf{k}) = O(\mathbf{k} - \mathbf{k}_m)$ in the Fourier domain, where $\mathbf{k} = (k_x, k_y)$ denotes the 2D Fourier space coordinates and $\mathbf{k}_m = (k_{mx}, k_{my})$ is the 2D wavevector of the plane wave illumination of the m th LED. After passing through an imaging system with the transfer function $P(\mathbf{k})$, the m th intensity image i_m from the sensor can be modeled as follows:

$$i_m(\mathbf{r}) = |\mathcal{F}^{-1}(O(\mathbf{k} - \mathbf{k}_m) \cdot P(\mathbf{k}))|^2 \quad (1)$$

It should be noted that the image from the sensor i_m in eq 1 corresponds to the intensity of the field, which indicates the loss in phase information in the object. The FPM reconstruction algorithm alternatively projects the estimated HR object information to an estimated LR image and vice versa. During this process, the captured image sequences are utilized as image-space intensity constraints to the estimated LR images and the extent of the pupil function (NA) is used as the Fourier domain constraint.²⁵ As a result, the complex field of the object $o(\mathbf{r})$ in a higher resolution as well as the complex pupil function can be recovered, $P(\mathbf{k})$.

In a typical FPM system, a 2D LED array is utilized to provide varying illumination angles for resolution improvement. In portable microscopy, LED arrays have also been used as external illumination sources with additional batteries and

associated microcontrollers for programmable illumination.^{7,8} In our work, we use the OLED display screen of the smartphone as the programmable illumination for the FPM, where a bright dot moving across the screen is displayed as illumination for each LR image capture. The OLED screens have high brightness and on–off contrast; moreover, they are highly programmable, making them suitable as an illumination source in computational microscopy.²⁶ Furthermore, the emission spectra of the OLEDs are close to the RGB LEDs used in typical FPMs, and the display pixels are sufficiently small to satisfy spatial coherence conditions at a smaller sample-to-illumination distance. The use of the screen as the illumination source eliminates the need for an additional LED array module and allows for the form factor of the entire system to be smaller, while simultaneously providing a large degree of freedom for illumination engineering.

To use the camera module and the display of a smartphone for FPM, we designed a customized microscope optics module using the Zemax Opticstudio software. Our prototype device is designed for a Google Pixel 3 XL smartphone, which has a built-in front camera module with an 8-megapixel image sensor (3264×2448 pixels) and a pixel size of $1.14 \mu\text{m}$, as well as a f/2.2 lens module with a focal length of 3.3 mm. Since the exact design of the lens module is proprietary information, we referred to the published patent of specific smartphone camera modules²⁷ for the optical design. The objective lens and overall magnification of the system were selected to maximize the FOV while still satisfying the sampling criterion of the image sensor. We selected an off-the-shelf M12 miniature camera lens (f/5.6) as the objective lens, which had an equivalent NA of 0.09 and expected resolution of $3.5 \mu\text{m}$. Meanwhile, we selected an overall magnification of $1.56\times$ for the microscope such that a single superpixel (2×2 sensor pixels) in the image sensor samples the Airy disc of the microscope at above the Nyquist sampling rate, resulting in an imaging FOV of $2.1 \times 1.6 \text{ mm}^2$.²⁸

The optical design of the microscope is shown in Figure 2. Here, two mirrors were placed in the optical path to use the display and the camera module on the front face of the smartphone in the transillumination scheme. Meanwhile, a tube lens and an eyepiece lens were utilized to relay the object plane to the image sensor with a field-lens placed in the intermediate image plane to match the pupils of the objective lens and the smartphone camera module. With this design, we were able to use the entire region of the sensor with minor vignetting and aberrations. Subsequently, a 3D-printed housing

was designed to secure all the optical components as well as the smartphone and the sample in place. A low-cost linear stage and a slide holder can be mounted for focusing and holding the sample. The list of the entire parts and the microscope design file are provided in the **Supporting Information, S1 and S6**. It should be noted that all the components used in the design were inexpensive off-the-shelf parts rather than custom or high-end optics. The overall size of the microscope module is $9 \times 11 \times 11 \text{ cm}^3$, and its weight is 400 g without the smartphone.

The use of the screen as the illumination source not only makes the entire system simple and compact but also provides a large degree of freedom for illumination engineering. To effectively recover the object information using the FP reconstruction algorithm, every point source should uniformly illuminate the sample with the same power.²⁹ However, the intensity of the incident light to the sample varies depending on the illumination angle, which is due to the increment in the propagation distance and viewing angle of the display. The small pixel size and programmability of the display screen can be useful as the size of the bright dots can be easily adjusted for the larger angles of illumination as a function of the propagation distance and viewing angle (Figure 3a). We

illumination. Ideally, the illumination should satisfy $\theta_s \ll \theta_p$ to meet the spatial coherence condition, where θ_s denotes the angular extent of the illumination source and θ_p denotes the NA of the imaging system.³¹ In our settings, $\theta_s = 0.03$ and $\theta_p = 0.09$ and was thus within the partially coherent illumination regime, as was the case in a number of previous FPM studies that utilized millimeter-sized LEDs for the illumination.^{32,33} In consideration of this partial coherence effect, we used apodized pupil constraints throughout our image reconstruction algorithm, as was suggested in ref 34.

To obtain LR images, the smartphone captures and saves images from the front camera module where the microscope is mounted, in sync with the illumination pattern on the display where the bright dot is moving. In our experiments, we used a total of 69 LR images with a maximum illumination NA of 0.29. As a result, the expected resolution of the microscope was $0.83 \mu\text{m}$ with a synthetic NA of 0.38, which is the sum of the illumination and objective NA. In our prototype, the maximum achievable NA is limited by the sensitivity of the camera and the signal-to-noise ratio (SNR) of the LR images. In most biological samples, LR images captured at a higher angle of illumination with a moderate exposure time are too noisy and have no significant contribution to the recovery of the outer region of the Fourier spectrum of the object where the signal itself is very low.

The recovery of the HR image follows the standard FP reconstruction algorithm^{15,35} with the EPRY used for aberration correction.¹⁸ In the FP reconstruction process, accurate knowledge of the angle of each illumination is crucial because any small error in the illumination wavevector (k_m) will induce severe artifacts and result in image resolution degradation. However, in conventional FPM settings using LED arrays, the exact angle may be inaccurate due to the misalignment of the system and displacement of each element in the LED array. To correct for such errors, various software calibration methods involving the use of the LR image information have been proposed, which include the identification of the exact angle of illumination from the Fourier spectrum³⁶ and joint optimization for the degree of misalignment during the FP reconstruction.³⁷ While our smartphone FPM is less prone to misalignment errors, the exact angles of illuminations as a function of lateral position on the object must be precisely calculated to reconstruct HR images over the full FOV.

In our smartphone FPM, the FOV size is relatively large for the aperture size and focal lengths of the optics compared with that of conventional FPM, indicating that the CRA and actual illumination wavevectors significantly vary across the FOV. For the FP reconstruction, we compute for a small segment (200 pixels \times 200 pixels) of the LR images at a time considering the coherence area of the illumination.¹⁵ For this region of interest (ROI) in the LR image, the exact position along the object plane in reference to the optical axis and corresponding angle of illuminations for all LR images needs to be precomputed. Here, we first corrected for the pincushion distortion of the captured LR images using precalibrated coordinate transformation³⁸ and then calculated the actual position using the magnification of the microscope (Figure 3c,d). Subsequently, considering the screen-to-sample distance and the actual pixel positions of the illumination dots on the screen, we computed for the illumination wavevectors with respect to the CRA at the object position, as determined by the front focal length of the objective lens (Figure 3a,e). This simple precalculation of the

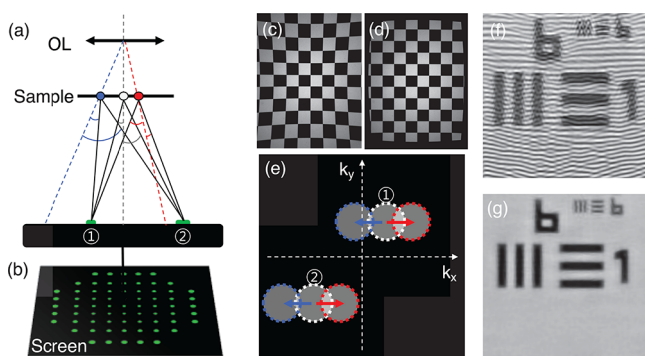


Figure 3. (a) Illustration demonstrating the variations in the illumination wavevector at different positions on the sample plane (OL, objective lens). (b) Illumination dot patterns used in our device. Each dot is turned on one at a time for LR image capture. (c) Full-field image of a checkerboard target showing pincushion distortion of the microscope. (d) Distortion-corrected image for illumination angle calibration and image reconstruction. (e) Wavevector corrections in the Fourier space for the sample positions marked in panel a. (f, g) Image reconstruction result before (f) and after (g) applying the distortion and angle corrections shown in panels a–e.

precompute the factor of increment as a function of the illumination angle and as the user sets the reference dot size (at center), the step size, and the number of illumination scans (Figure 3), the corresponding dot sizes for the illumination sequence are automatically applied. The screen pattern used in our demonstration could easily replace the customized dome LED arrays⁷ and potentially the other illumination patterns that have been suggested for improving imaging speed and reconstruction quality in FPM.^{19,21,30}

Considering the brightness of the screen, we set the sample-to-screen distance to 25 mm. In our experiments, a series of images of a single bright dot with a radius of 15 display pixels (at the center) moving across the screen was utilized as the FPM illumination source, which required a camera exposure time of 300 ms. In the FP reconstruction, the single LED illumination is generally modeled as a spatially coherent

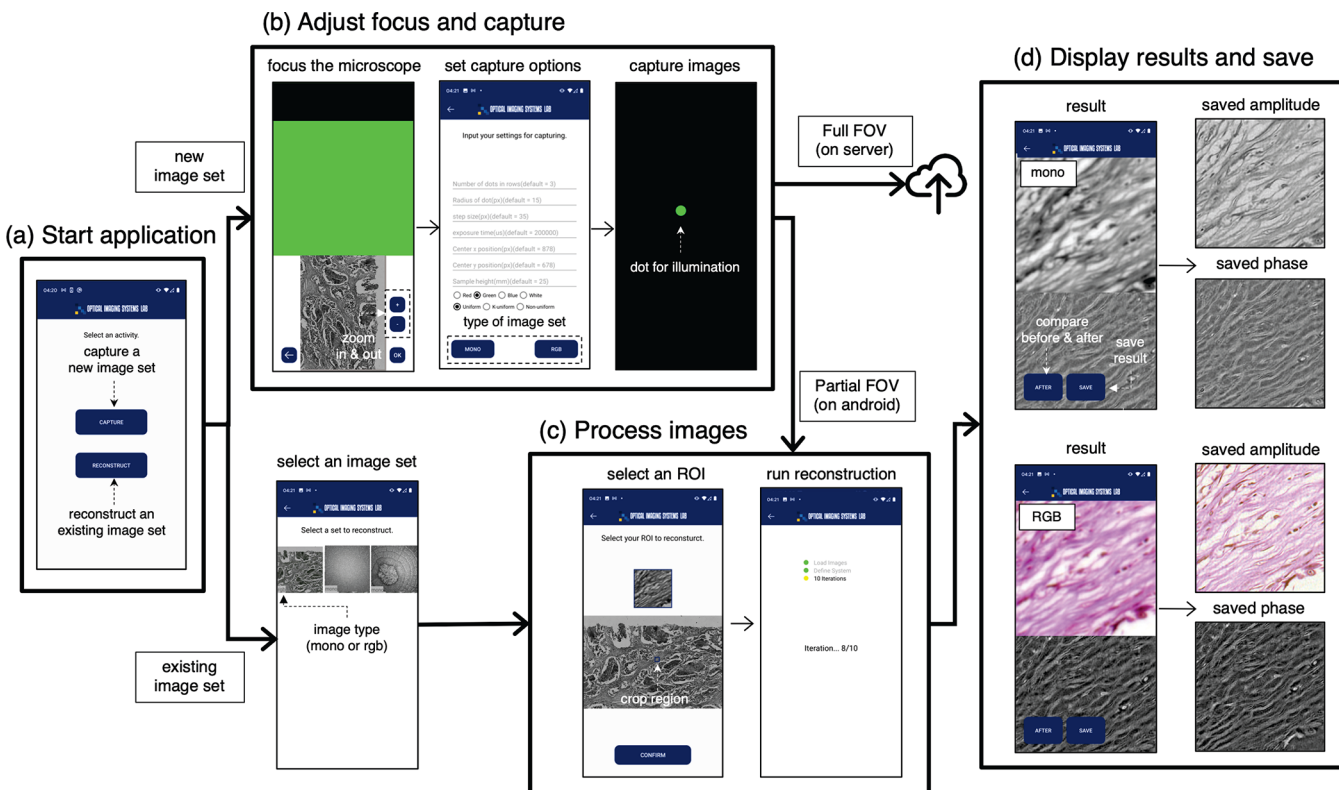


Figure 4. Workflow of our Android application for image capture, FPM reconstruction, and display of the resulting image.

illumination wavevectors effectively eliminated the reconstruction artifacts in the final HR images (Figure 3f,g), without the use of the iterative calibration algorithms generally employed in conventional FPM.

We developed a customized Android application that performs the entire process of image acquisition, reconstruction, and display of the images on the smartphone. The workflow of our Android applications is presented in Figure 4 and is described below:

- (1) Load sample and adjust the focus using the preview image.
- (2) Enter the parameters for image capture. If not entered, the default settings are used.
- (3) A sequence of LR images is captured and saved on the device.
- (4) Confirm the captured images and select the ROI for reconstruction.
- (5) Run *in situ* calculations for resolution enhancement on the smartphone.
- (6) The reconstructed HR images are displayed and saved on the smartphone.

The application mainly consists of three activities, namely, capture, reconstruction, and display. The capture activity begins with the sample loading step, where the users can adjust the focus of the sample and at the same time observe the camera preview located at the bottom half of the screen while the upper part of the screen illuminates the sample. Then, the images are captured using the assigned capture settings, in sync with each illumination pattern with a moving dot position, and are then saved on the smartphone storage in JPEG format. While some smartphones support saving the uncompressed 10-bit raw images, the loading and processing of raw files can be slow, without a great deal of gain in terms of image quality

(See section 2 in the *Supporting Information* for a comparison). Thus, we used JPEG compressed images in all our experiments. The exposure time was set between 200 and 300 ms to maximize the dynamic range of the images, with a total time of 1 min for capturing 69 images (Figure 4b). In terms of color imaging, three sets of LR images are captured with a sequence of red, green, and blue dots displayed on the screen, whereas only green illumination is used for monochromatic imaging.

For in-app FP reconstruction, users can select the current image set or load a previously captured image set before selecting a ROI for HR imaging. Once a ROI is selected, the app loads the entire LR image sequence in the memory, selects the ROI, and performs the FP reconstruction for ten iterations to ensure convergence.³⁵ Finally, both the amplitude and phase images of the recovered complex object are displayed on the screen as presented in Figure 4. Here, an ROI of 200×200 can be reconstructed in a total of 30 s on a Google Pixel 3 XL, which includes 20 s of image loading (See *Supplementary Movie*). Once the LR images are loaded on the device's memory, reconstructing (or zooming into) different ROIs would require 10 s of computing time per ROI. To further improve this speed, options for parallel reconstruction on the smartphone device as well as remote reconstruction on the server are available. The total processing times for full FOV (3200×2000 pixels) are ~ 850 s and ~ 150 s for on-device and remote reconstruction, respectively, which include file input/output and transfer times (See section 5 in *Supporting Information*).

For color reconstruction, we capture images with sequential RGB illumination to avoid any possible artifacts from demosaicing in the JPEG images and to maximize the signal-to-noise ratio of raw images (See *Supporting Informa-*

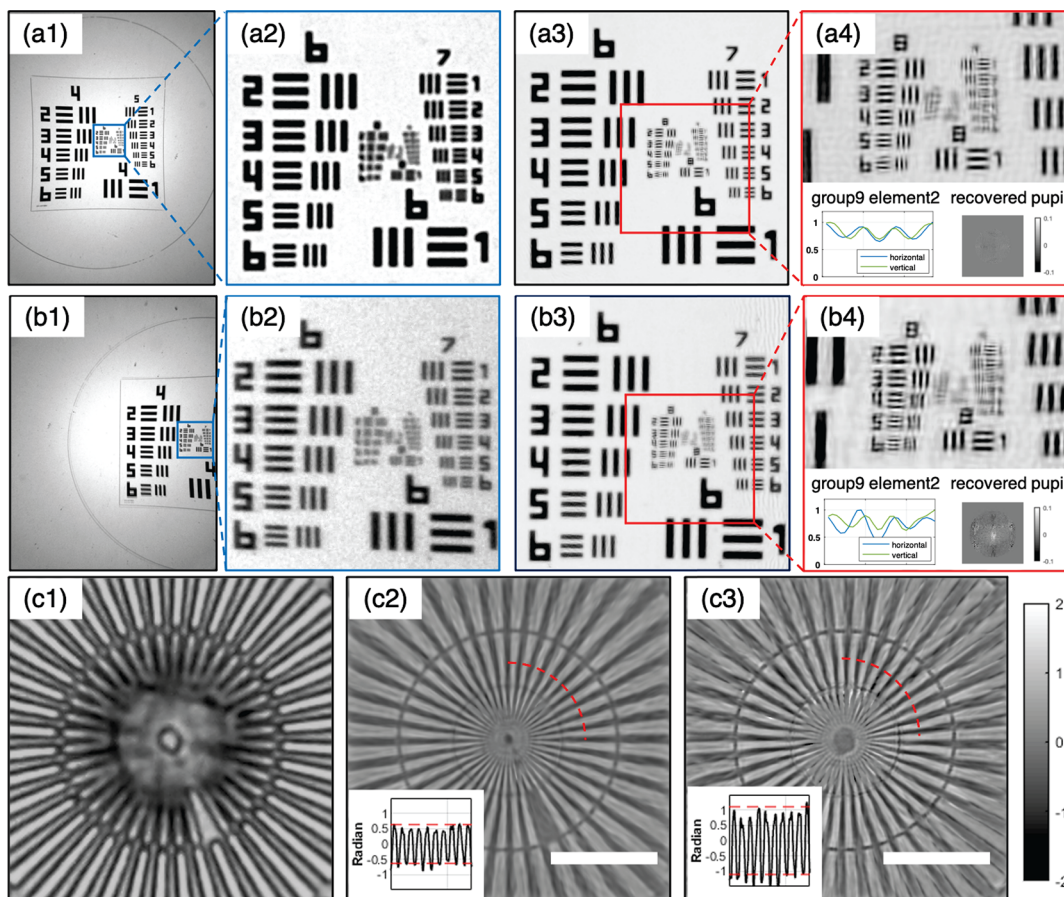


Figure 5. FP reconstruction performance of our smartphone microscope. (a) Quantification of resolution enhancement at the center of the FOV. (b) Quantification of resolution enhancement at the edge of the FOV. Raw images (a1, a2, b1, b2) and reconstructed amplitude including line plot of group 9 element 2 and recovered pupil function (a3, a4, b3, b4). (c) Verification of phase imaging capabilities: (c1) raw image of phase target with partially coherent illumination; (c2) reconstruction of 200 nm feature height phase target; (c3) reconstruction of 350 nm feature height phase target. The phase delay for 200 nm feature height with $n = 1.52$ is 1.2 and that for 350 nm feature height is 2.20. The scale bar indicates 50 μm .

tion, section 3). Then each color image is reconstructed separately using the corresponding color channel from each capture. However, we designed an algorithm to load and process three color channels in parallel; thus, the required capture and file I/O time is $3\times$ longer than the monochromatic images, but the reconstruction time is the same as that for monochromatic images.

RESULTS AND DISCUSSION

We first verified the resolution enhancement of our smartphone FPM using standard resolution targets. As presented in Figure 5a1,a2, no features above group 7 element 4 of the US Air Force resolution target are resolved in LR images before applying FP reconstruction, indicating an initial half-pitch resolution of 2.76 μm . After FP reconstruction, a group 9 element 2 with 870 nm line widths can be resolved (Figure 5a3,a4), indicating a more than 3-fold improvement in optical resolution. A submicrometer resolution is sufficient for observing subcellular structures in histology and cytology samples and is thus suitable for clinical applications in the field.

The image quality at the edge of the microscope's FOV is presented in Figure 5b. While more optical aberrations were initially present in the outer FOV, the EPRY algorithm recovered the pupil function at each ROI and produces aberration-corrected images. Furthermore, the distortion correction and precalculated wavevectors produced HR images

without misalignment artifacts, even at the far ends of the field. The reconstructed HR images in Figure 5b3,b4 show the same line pairs placed at the right horizontal end of the FOV, where the first two elements in the group 9 can still be resolved with lower contrast and more errors compared to the center of the field.

Considering the half-pitch resolution of our system, the equivalent NA is 0.38 and the SBP of our system is ~ 18 megapixels with a total FOV of $\sim 3.4 \text{ mm}^2$. Comparatively, a regular 0.4 NA 20 \times microscope objective lens has a SBP of ~ 6 megapixels and most published smartphone-attached microscopes achieved a SBP of less than a few megapixels (See Supporting Information, section 4). This means that our device can be effective in image-based screening and diagnostic applications, where a large number of samples over a large area need to be scanned in high throughput.

We also verified the phase imaging capabilities of our smartphone FPM. While the phase information on the object is lost during the image acquisition process in a regular microscope, FPM utilizes the data redundancy between the adjacent captured images and recovers the entire complex field of the object using the iterative phase retrieval algorithm. Two spoke-patterned phase targets, with feature heights of 200 and 350 nm and a refractive index of 1.52 were imaged and processed using our device. The recovered phase images of the two phase targets show improved spatial resolution compared

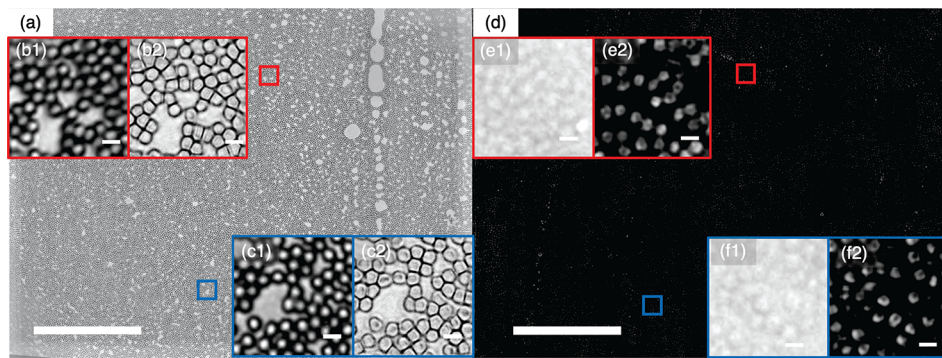


Figure 6. FP reconstruction result for unstained blood smear sample. (a) Full FOV image of the reconstructed amplitude of dry blood smear. (d) Full FOV reconstructed phase image of blood smear immersed in oil. The insets show raw images (left, b1, c1, e1, f1) and the reconstructed amplitude/phase images (right, b2, c2, e2, f2) corresponding to the ROI marked in panels a and d. The scale bar is 500 μm for the full FOV reconstructed amplitude and phase and 10 μm in the insets.

with the LR images, with the two targets showing different quantitative phase retardation of ± 0.5 and ± 1 rad, as presented in the inset of Figure 5c.

Next, we applied our system to observe various biological samples. Here, we imaged an unstained dry blood smear, a typical clinical sample used in the field requiring a high SBP for the screening of blood-borne diseases. As shown in Figure 6a, a FOV of $2.1 \times 1.6 \text{ mm}^2$ can be imaged in HR using our device. The FP reconstruction reveals sharper features of the red blood cells in the final amplitude images compared with the raw images (Figure 6b,c). We also performed phase imaging of an unstained blood film immersed in oil (refractive index 1.5). As shown in Figure 6b, the phase images of the blood film successfully reveal the concave disc shape of red blood cells. However, the spatial resolution of the recovered phase images appears worse than that of the amplitude images of dry blood film in Figure 6. The decrement in the refractive index differences between the cells and surrounding medium in the oil-immersed film causes less scattering from the sample, leading to a low contrast in the raw images as presented in Figure 6e1,f1. The effect of the reduced scattering from the sample is more prominent at larger illumination angles where the SNR is lower. As a result, the spatial frequency extent of the recovered images and the final spatial resolution is restricted by the low SNR of the acquired images, which is also highly sample-dependent. This problem can be mitigated by the use of longer exposure times in the image sensor and brighter illuminations, which is also potentially achievable with multiplexed FPM imaging.¹⁹

To demonstrate the color imaging capability of our smartphone FPM, we imaged two biological samples: a stained cross-section of a *Tilia* plant stem and a stained Papanicolaou (Pap) smear sample of human cervical epithelial cells. For color FPM imaging, each color channel is captured and reconstructed separately and then combined into a color image following a normalization step. Figure 7a presents the full FOV reconstruction result of the *Tilia* stem, which shows the vascular bundle in the secondary xylem, as well as the stained cell nuclei in the pith and phloem of the stem. We also obtained full FOV color images of Pap smear slides of human cervical epithelial cells with our device. Pap smear cytology is currently the standard screening test for cervical cancer, which is often unavailable in remote areas of developing countries. Here, portable FPM could provide a cost-effective and reliable tool for cytological screening and histopathology in remote

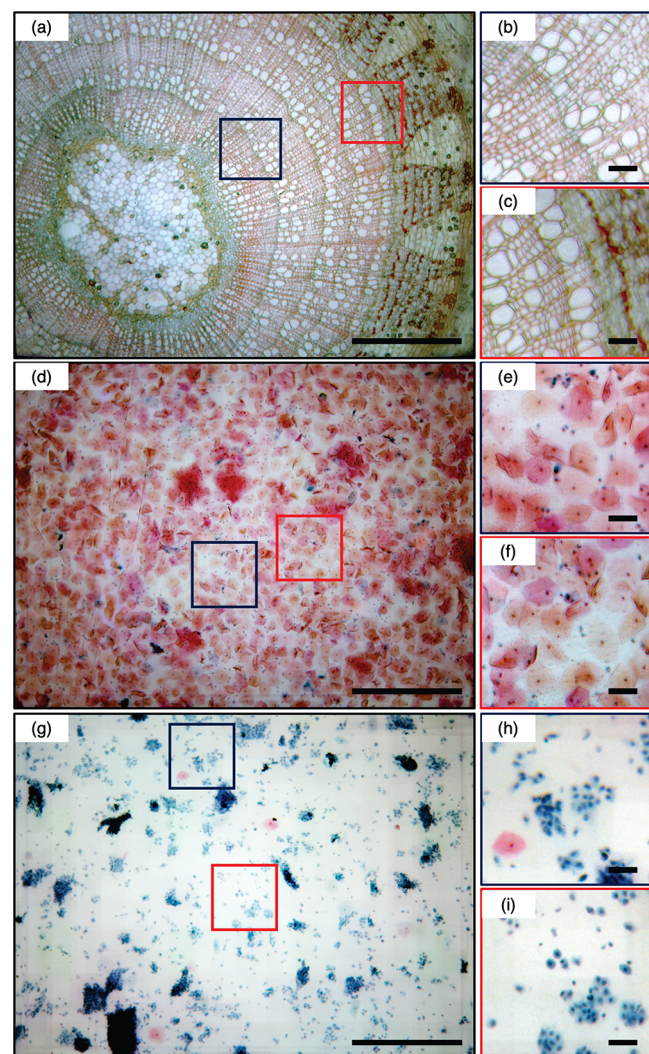


Figure 7. (a) Full FOV color reconstruction result of cross-section of a *Tilia* stem. Magnified images with regions indicated by blue box (b) and red box (c). (d) Full FOV color reconstruction result of Pap smear with superficial cells. Magnified images with regions boxed in blue (e) and red (f). (g) Full FOV color reconstruction result of Pap smear with parabasal squamous cells. Magnified images with regions marked with blue box (h) and red box (i). The scale bar is 500 μm for panels a, d, and g and 50 μm for panels b, c, e, f, h, and i.

laboratories. In Figure 7d–i, the reconstructed color images of the Pap smear slides show the superficial cells stained in red and the parabasal cells stained in blue, with sufficient resolution to visualize the cell nuclei.

CONCLUSION

In this work, we demonstrated a low-cost smartphone microscope that can achieve submicrometer resolution over a wide FOV of $2.1 \times 1.6 \text{ mm}^2$ surpassing the SBP of conventional microscopes. We have implemented an FPM on a smartphone using the display screen as a programmable illumination source, without any external light sources or modification of the device. The microscope module was constructed using low-cost optics and 3D-printed parts, which allow for cost-effective deployment of our imaging system in field settings. Moreover, we developed an Android application to capture and recover images on the mobile device even in a situation where a network connection is not available. Meanwhile, we devised the illumination angle correction method for a reliable and fast FP reconstruction on the mobile device without additional computational steps for calibrations. The imaging performance for both bright-field and phase microscopy was demonstrated, using standard targets and biological samples.

In addition to the improved form-factor of FPM, we believe that our work presents a number of technical aspects that can contribute to the field of computational microscopy while leaving some room for future research. Specifically, our work presents the possibility of using a high-density OLED display module for programmable illumination in computational microscopy that can be easily randomized, multiplexed, and optimized for optimal image reconstruction. For example, FP illuminations for uniform wavevector spacing or low-frequency-weighted sampling can be easily realized by displaying precomputed patterns on the screen, as opposed to the customized LED arrays utilized in previous works.^{7,29} Multiplexed and more complex illumination could potentially improve the image quality obtained using our smartphone FPM, where the final resolution is limited by the SNR of the LR images. Learning-based approaches to find optimal sampling patterns for specified tasks²¹ could also be further explored with the screen illumination in a follow-up study. Second, our method for illumination angle correction can be easily combined with other calibration methods in FPM to compensate for large variations in the CRA, especially for low-magnification FPM setups. We also believe that our system can be further improved with the use of state-of-the-art cameras and emerging display technologies, such as micro-LED displays. Moreover, the use of deep learning-based reconstruction models in place of the iterative FP algorithm could expedite the imaging process with a pretrained inference model running on advanced mobile processors. As global health issues continue to persist and new epidemic challenges arise, we believe that our smartphone microscopy technology can effectively address the clinical needs in point-of-care environments.

ASSOCIATED CONTENT

Supporting Information

The Supporting Information is available free of charge at <https://pubs.acs.org/doi/10.1021/acsphtronics.1c00350>.

Instructions for building a smartphone-based Fourier ptychographic microscope module, comparison of the reconstruction results between DNG and JPEG formats, comparison between monochromatic and color multiplexed illuminations, comparison of the space-bandwidth product of smartphone-enabled microscopes, reconstruction speed of the smartphone FPM, and code availability ([PDF](#))

Supplementary movie demonstrating use ([MP4](#))

AUTHOR INFORMATION

Corresponding Author

Seung Ah Lee – School of Electrical and Electronic Engineering, Yonsei University, Seoul 03722, South Korea;
ORCID: [0000-0001-5173-1565](https://orcid.org/0000-0001-5173-1565); Email: seungahlee@yonsei.ac.kr

Authors

Kyung Chul Lee – School of Electrical and Electronic Engineering, Yonsei University, Seoul 03722, South Korea;
ORCID: [0000-0002-5533-3078](https://orcid.org/0000-0002-5533-3078)

Kyungwon Lee – School of Electrical and Electronic Engineering, Yonsei University, Seoul 03722, South Korea

Jaewoo Jung – School of Electrical and Electronic Engineering, Yonsei University, Seoul 03722, South Korea

Se Hee Lee – Department of Computer Science, Yonsei University, Seoul 03722, South Korea

Donghyun Kim – School of Electrical and Electronic Engineering, Yonsei University, Seoul 03722, South Korea;
ORCID: [0000-0003-1960-0527](https://orcid.org/0000-0003-1960-0527)

Complete contact information is available at:
<https://pubs.acs.org/10.1021/acsphtronics.1c00350>

Notes

The authors declare no competing financial interest.

ACKNOWLEDGMENTS

This work was supported by the National Research Foundation of Korea (NRF) grant funded by the Korea government (No.2019R1A4A1025958) and by Veraverse Inc. The authors would like to thank Dr. Eunhyang Park for the help with the clinical Pap smear samples.

REFERENCES

- (1) Breslauer, D. N.; Maamari, R. N.; Switz, N. A.; Lam, W. A.; Fletcher, D. A. Mobile phone based clinical microscopy for global health applications. *PLoS One* **2009**, *4*, e6320.
- (2) Switz, N. A.; D'Ambrosio, M. V.; Fletcher, D. A. Low-cost mobile phone microscopy with a reversed mobile phone camera lens. *PLoS One* **2014**, *9*, e95330.
- (3) Kobori, Y.; Pfanner, P.; Prins, G. S.; Niederberger, C. Novel device for male infertility screening with single-ball lens microscope and smartphone. *Fertil. Steril.* **2016**, *106*, 574–578.
- (4) Tseng, D.; Mudanyali, O.; Oztoprak, C.; Isikman, S. O.; Sencan, I.; Yaglidere, O.; Ozcan, A. Lensfree microscopy on a cellphone. *Lab Chip* **2010**, *10*, 1787–1792.
- (5) Lee, S. A.; Yang, C. A smartphone-based chip-scale microscope using ambient illumination. *Lab Chip* **2014**, *14*, 3056–3063.
- (6) Dai, B.; Jiao, Z.; Zheng, L.; Bachman, H.; Fu, Y.; Wan, X.; Zhang, Y.; Huang, Y.; Han, X.; Zhao, C.; et al. Colour compound lenses for a portable fluorescence microscope. *Light: Sci. Appl.* **2019**, *8*, 75.
- (7) Phillips, Z. F.; D'Ambrosio, M. V.; Tian, L.; Rulison, J. J.; Patel, H. S.; Sadras, N.; Gande, A. V.; Switz, N. A.; Fletcher, D. A.; Waller,

- L. Multi-contrast imaging and digital refocusing on a mobile microscope with a domed led array. *PLoS One* **2015**, *10*, e0124938.
- (8) Jung, D.; Choi, J.-H.; Kim, S.; Ryu, S.; Lee, W.; Lee, J.-S.; Joo, C. Smartphone-based multi-contrast microscope using color-multiplexed illumination. *Sci. Rep.* **2017**, *7*, 7564.
- (9) Pfeil, J.; Dangelat, L. N.; Frohme, M.; Schulze, K. Smartphone based mobile microscopy for diagnostics. *Journal of Cellular Biotechnology* **2019**, *4*, 57–65.
- (10) Ozcan, A. Mobile phones democratize and cultivate next-generation imaging, diagnostics and measurement tools. *Lab Chip* **2014**, *14*, 3187–3194.
- (11) Dong, S.; Guo, K.; Nanda, P.; Shiradkar, R.; Zheng, G. FPscope: a field-portable high-resolution microscope using a cellphone lens. *Biomed. Opt. Express* **2014**, *5*, 3305–3310.
- (12) de Haan, K.; Ceylan Koydemir, H.; Rivenson, Y.; Tseng, D.; Van Dyne, E.; Bakic, L.; Karinca, D.; Liang, K.; Ilango, M.; Gumustekin, E.; Ozcan, A. Automated screening of sickle cells using a smartphone-based microscope and deep learning. *npj Digital Medicine* **2020**, *3*, 76.
- (13) Im, H.; Castro, C. M.; Shao, H.; Liang, M.; Song, J.; Pathania, D.; Fexon, L.; Min, C.; Avila-Wallace, M.; Zurkiya, O.; et al. Digital diffraction analysis enables low-cost molecular diagnostics on a smartphone. *Proc. Natl. Acad. Sci. U. S. A.* **2015**, *112*, 5613–5618.
- (14) Rivenson, Y.; Ceylan Koydemir, H.; Wang, H.; Wei, Z.; Ren, Z.; Gunaydin, H.; Zhang, Y.; Gorocs, Z.; Liang, K.; Tseng, D.; et al. Deep learning enhanced mobile-phone microscopey. *ACS Photonics* **2018**, *5*, 2354–2364.
- (15) Zheng, G.; Horstmeyer, R.; Yang, C. Wide-field, high-resolution Fourier ptychographic microscopy. *Nat. Photonics* **2013**, *7*, 739–745.
- (16) Tian, L.; Waller, L. Quantitative differential phase contrast imaging in an LED array microscope. *Opt. Express* **2015**, *23*, 11394–11403.
- (17) Ou, X.; Horstmeyer, R.; Yang, C.; Zheng, G. Quantitative phase imaging via Fourier ptychographic microscopy. *Opt. Lett.* **2013**, *38*, 4845–4848.
- (18) Ou, X.; Zheng, G.; Yang, C. Embedded pupil function recovery for Fourier ptychographic microscopy. *Opt. Express* **2014**, *22*, 4960–4972.
- (19) Tian, L.; Liu, Z.; Yeh, L.-H.; Chen, M.; Zhong, J.; Waller, L. Computational illumination for high-speed in vitro Fourier ptychographic microscopy. *Optica* **2015**, *2*, 904–911.
- (20) Cheng, Y. F.; Strachan, M.; Weiss, Z.; Deb, M.; Carone, D.; Ganapati, V. Illumination pattern design with deep learning for single-shot Fourier ptychographic microscopy. *Opt. Express* **2019**, *27*, 644–656.
- (21) Muthumbi, A.; Chaware, A.; Kim, K.; Zhou, K. C.; Konda, P. C.; Chen, R.; Judkewitz, B.; Erdmann, A.; Kappes, B.; Horstmeyer, R. Learned sensing: jointly optimized microscope hardware for accurate image classification. *Biomed. Opt. Express* **2019**, *10*, 6351–6369.
- (22) Jiang, S.; Guo, K.; Liao, J.; Zheng, G. Solving Fourier ptychographic imaging problems via neural network modeling and TensorFlow. *Biomed. Opt. Express* **2018**, *9*, 3306–3319.
- (23) Konda, P. C.; Loetgering, L.; Zhou, K. C.; Xu, S.; Harvey, A. R.; Horstmeyer, R. Fourier ptychography: current applications and future promises. *Opt. Express* **2020**, *28*, 9603–9630.
- (24) Zheng, G.; Shen, C.; Jiang, S.; Song, P.; Yang, C. Concept, implementations and applications of Fourier ptychography. *Nature Reviews Physics* **2021**, *3*, 207.
- (25) Fienup, J. R. Reconstruction of an object from the modulus of its Fourier transform. *Opt. Lett.* **1978**, *3*, 27–29.
- (26) Zheng, G.; Lee, S. A.; Antebi, Y.; Elowitz, M. B.; Yang, C. The ePetri dish, an on-chip cell imaging platform based on subpixel perspective sweeping microscopy (SPSM). *Proc. Natl. Acad. Sci. U. S. A.* **2011**, *108*, 16889–16894.
- (27) Samsung Electro-Mechanics Co. Lens module, US20160124189 A1. 2018.
- (28) Aidukas, T.; Eckert, R.; Harvey, A. R.; Waller, L.; Konda, P. C. Low-cost, sub-micron resolution, wide-field computational microscopy using opensource hardware. *Sci. Rep.* **2019**, *9*, 7457.
- (29) Guo, K.; Dong, S.; Nanda, P.; Zheng, G. Optimization of sampling pattern and the design of Fourier ptychographic illuminator. *Opt. Express* **2015**, *23*, 6171–6180.
- (30) Xue, Y.; Cheng, S.; Li, Y.; Tian, L. Reliable deep-learning-based phase imaging with uncertainty quantification. *Optica* **2019**, *6*, 618–629.
- (31) Goodman, J. W. *Introduction to Fourier optics*; W.H. Freeman, 2017; pp 186–194.
- (32) Horstmeyer, R.; Chen, R. Y.; Ou, X.; Ames, B.; Tropp, J. A.; Yang, C. Solving ptychography with a convex relaxation. *New J. Phys.* **2015**, *17*, 053044.
- (33) Dong, S.; Shiradkar, R.; Nanda, P.; Zheng, G. Spectral multiplexing and coherent-state decomposition in Fourier ptychographic imaging. *Biomed. Opt. Express* **2014**, *5*, 1757–1767.
- (34) Chen, X.; Zhu, Y.; Sun, M.; Li, D.; Mu, Q.; Xuan, L. Apodized coherent transfer function constraint for partially coherent Fourier ptychographic microscopy. *Opt. Express* **2019**, *27*, 14099–14111.
- (35) Yeh, L.-H.; Dong, J.; Zhong, J.; Tian, L.; Chen, M.; Tang, G.; Soltanolkotabi, M.; Waller, L. Experimental robustness of Fourier ptychography phase retrieval algorithms. *Opt. Express* **2015**, *23*, 33214–33240.
- (36) Eckert, R.; Phillips, Z. F.; Waller, L. Efficient illumination angle self-calibration in Fourier ptychography. *Appl. Opt.* **2018**, *57*, 5434–5442.
- (37) Sun, J.; Chen, Q.; Zhang, Y.; Zuo, C. Efficient positional misalignment correction method for Fourier ptychographic microscopy. *Biomed. Opt. Express* **2016**, *7*, 1336–1350.
- (38) Zhang, Z. A flexible new technique for camera calibration. *IEEE Transactions on Pattern Analysis and Machine Intelligence* **2000**, *22*, 1330–1334.